International Journal of Fracture **212:** 87–98, 2001.

Dynamic fracture of tungsten base heavy alloys

D. RITTEL and G. WEISBROD
Faculty of Mechanical Engineering, Technion, Haifa 32000, Israel; e-mail: merittel@tx.technion.ac.il

Received 14 February 2000; accepted in revised form 13 June 2001

Abstract. A recently developed short beam experimental technique has been applied to the characterization of the mode I dynamic fracture toughness (KId) of a commercial tungsten base heavy alloy (w/o-90W-7Ni-3Fe). The specimens were taken from a cylindrical swaged alloy bar and tested at a typical loading rate of the order of 10^6 MPa$\sqrt{\text{m}}/s$. Three different crack orientations (one longitudinal and two radial) were investigated. The *KId* values obtained for the three crack orientations are compared with the corresponding values obtained under quasi-static loading conditions (KIc). Our results show that the dynamic fracture of heavy alloys is *both anisotropic and rate sensitive*. For specimens containing radial cracks (LR, RR), the dynamic fracture toughness is *higher* that its static counterpart. By contrast, for longitudinal cracks (RL), the dynamic fracture toughness is *lower* than the static one. Also, for radial cracks, both the (average) static and the dynamic fracture toughness are higher than in the longitudinal orientation. These new results about the anisotropy of the dynamic fracture toughness of the heavy alloys are reported and correlated with metallographic and fractographic examinations.

Key words: Anisotropy, dynamic fracture, fracture toughness, one point impact, short beam, tungsten base heavy alloy.

1. Introduction

Tungsten base heavy alloys are particulate reinforced composites, which are produced by a liquid phase sintering process (Gurwell et al., 1984). These alloys exhibit a good combination of strength and ductility, which has been extensively studied in the past (see, e.g., Krock and Shepard, 1963; Churn and German, 1984; Rittel and Roman, 1986). Typical applications of these alloys take advantage of their high density (typically 17000 kg m^{-3}), such as inertial balancing systems and high energy kinetic penetrators. The quasi-static fracture properties of these alloys have been studied to limited extent, and a wide range of fracture toughness values (32 MPam$^{1/2}$–234 MPam$^{1/2}$) can be found in the literature, according to the composition and thermomechanical treatment of the alloy (for a review, see Ostolaza Zamora et al., 1992). The dynamic mechanical behavior of these materials has been studied at various strain rates using Kolsky bars (Woodward et al., 1985; Zurek and Gray, 1991; Ramesh and Coates, 1992; Kim et al., 1998) or explosive loading (Anderson et al., 1988). These studies show that the material is strain rate sensitive, as expected from the BCC tungsten component. The fractographic features have been well documented, and they reveal a wealth of details related to the specific failure mechanisms of these alloys (Churn and German, 1984; Rittel and Roman, 1986).

For many applications, the heavy alloys are manufactured in the form of long cylindrical bars which can be subsequently swaged, forged and heat treated. Therefore some degree of microstructural anisotropy is likely to develop, which in turn should influence the mechanical properties. Surprisingly enough, the issue of mechanical anisotropy has not been investigated to the best of our knowledge, specifically concerning fracture properties of the material. Furthermore, little data is available to date on the dynamic fracture toughness of these alloys.

Couque et al. (1992) investigated several heavy alloys and measured the static and dynamic fracture toughness of these materials They report a noticeable reduction in the fracture toughness as the loading rate is increased. In this work, a critical distance criterion was used to predict the fracture toughness. However, the authors do not address anisotropy issues. Hack (1991) investigated the relationship between the quasi-static stress intensity factor at initiation and the subsequent crack velocity, both in a commercial heavy alloy (Teledyne X21C), and in pure tungsten. The heavy alloy was manufactured as a cylindrical bar. Two different specimen orientations were considered, however anisotropy issues were not addressed in this work.

Consequently, the present paper is aimed at bringing new results about the fracture toughness of a representative commercial heavy tungsten base alloy, with emphasis on the following issues: static versus dynamic fracture toughness, anisotropy of these properties, and influence of the loading rate. The paper is organized as follows: first, the theoretical and experimental (methods and specimens) framework is described. Next, typical results for the static and dynamic fracture properties are shown, followed by a discussion and conclusion section.

2. Theoretical

Quasi-static fracture toughness measurements are usually carried out following the recommendations of ASTM standards (e.g., ASTM E399). These recommendations set the specimen dimensions and fatigue precracking procedure. There are no similar standards for dynamic fracture toughness testing. Therefore, concerning specimen size and requirements, the simplest solution is to apply the ASTM E399 requirements to the dynamic case in order to validate the results.

Let us consider now the fracture of an anisotropic linear elastic material (for a detailed treatment of the subject, see, e.g., Kanninen and Popelar, 1985; or Broberg, 1999). While the case of general anisotropic fracture is quite complicated, a noticeable simplification arises when symmetry properties are considered. For an orthotropic material with the crack lying in one plane of symmetry, the (mode I) energy release rate G_I is related to stress intensity factor K_I by the following simple expression:

$$G_I = K_I^2 \left(\frac{S_{11}S_{22}}{2}\right)^{1/2} \left[\left(\frac{S_{22}}{S_{11}}\right)^{1/2} + \frac{2S_{12} + S_{66}}{2S_{11}}\right]^{1/2}, \tag{1}$$

where S_{ij} are the components of the elastic compliance tensor. For the transversely isotropic case with respect to axis 3, $S_{11} = S_{22}$ and $S_{66} = 2(S_{11} - S_{12})$ (Nye, 1957). Equation (1) then reduces to the well-known expression obtained for the isotropic case.

The *procedure* for dynamic fracture toughness determination (*KId*) has been exposed in detail in Weisbrod and Rittel (2000) and will only be briefly outlined here. Basically, this procedure relies on the central assumption of the applicability of LEFM concepts. Therefore, the dynamic response of a cracked specimen to a unit impact, $\hat{K}_I(t)$, is first calculated as a reference. The evolution of the stress intensity is thus calculated as a convolution ($*$) between the applied load $F(t)$ and the above mentioned response. In other words:

$$K_I(t) = F(t) * \hat{K}_I(t). \tag{2}$$

The stress intensity factor is obtained from half the crack-tip opening $\hat{V}(t)$ as:

$$\hat{K}_I(t) = \frac{\hat{V}(t)E}{4(1-\nu^2)}\sqrt{\frac{2\pi}{r}}, \tag{3}$$

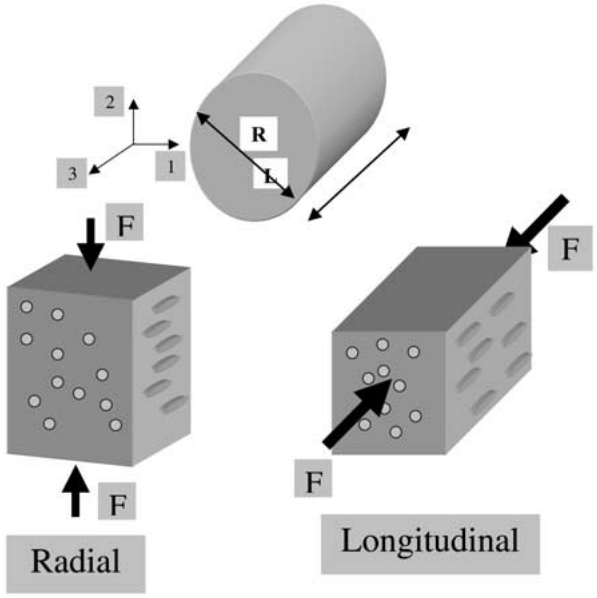

Figure 1. Orientation of the specimens for mechanical properties determination. The specimens are taken from a cylindrical bar. Grain flow has been schematically represented. F is the applied load.

where E is Young's modulus and r is the distance from the crack-tip.

Finally, the fracture toughness is identified as the value of the stress intensity factor at fracture time t_{frac}:

$$K_{Id} = K_I(t = t_{\text{frac}}). \tag{4}$$

Weisbrod and Rittel (2000) implemented these concepts in a series of one point impact experiments, using small precracked beams. The only boundary condition was the applied load, $F(t)$, and the fracture time was assessed using single wire fracture gages and miniature strain gages cemented in the vicinity of the crack-tip.

At this point, one must emphasize one more time that the above mentioned approach is strictly valid for stationary cracks subjected to transient loading, thus excluding any propagation related issues.

3. Experimental

3.1. Material

The experimental material was a commercial tungsten base heavy alloy (w/o-90W-7Ni-3Fe), whose density was found to be $\rho = 17100$ kg m^3. The experimental material was supplied as a cylindrical bar which had been slightly swaged by the manufacturer. Young's modulus and Poisson's ratio were determined for two orthogonal specimen orientations with respect to the applied load, as shown in Figure 1. The yield strength of the material is 1450 MPa, according to the manufacturer.

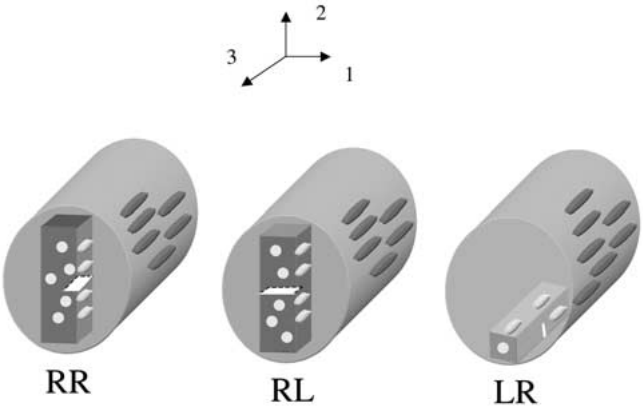

Figure 2. Dynamic fracture specimens. The orientation is indicated by two letters: the first indicates the specimen orientation (radial or longitudinal) and the second the direction of crack propagation.

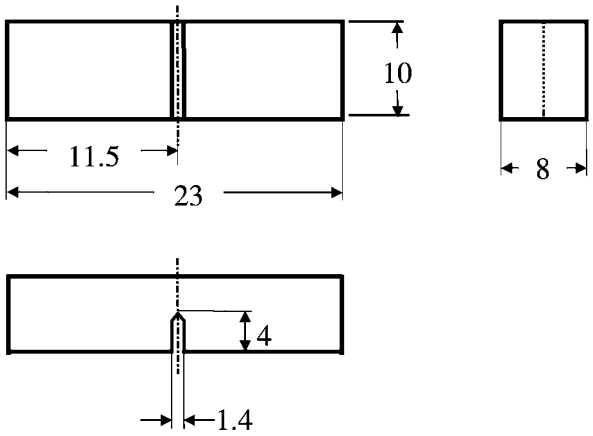

Figure 3. Dynamic fracture specimens (reprinted from Weisbrod and Rittel, 2000). All dimensions in mm. These specimens also served for static fracture toughness determination in the *LR* orientation.

3.2. SPECIMENS

Throughout the paper we will adopt the following convention: cracked specimens will be designated by two letters. The first indicates the orientation of the specimen (with the crack plane being perpendicular to the latter). The second letter indicates the direction of crack propagation. As an example, *LR* designates a *L*(ongitudinal) specimen with a crack in the basal plane (12) propagating in the *R*(adial) direction. The specimens are shown in Figure 2.

Compact tension specimens (12 mm thick) were machined from the rod for RR and RL crack orientations. For all the dynamic fracture toughness experiments and the LR static experiments, we used short cracked beams, whose geometry and dimensions are shown in Figure 3 (as in Weisbrod and Rittel, 2000). All the specimens were fatigue precracked on a servo-hydraulic machine (MTS-810), according to ASTM standard recommendations (ASTM-E399, 1993).

Table 1. Quasi-static fracture toughness – *KIc* – at two loading rates for each orientation. (The values have been rounded off to the nearest integer).

Crosshead velocity (mm min^{-1})	*RR* specimen ($MPam^{1/2}$)	*RL* specimen ($MPam^{1/2}$)	*LR* specimen ($MPam^{1/2}$)
0.5	70 ± 6	65 ± 8	60–61
10	71 ± 7	60 ± 4	67–74

4. Results

4.1. Elastic properties

Young's modulus was determined from the measured longitudinal wave velocity in the heavy alloy incident bar used for stress wave loading (e.g., along axis 3). This value represents the dynamic Young's modulus which is used in numerical calculations to accurately reproduce wave propagation in the specimen (Wada, 1992; Rittel and Maigre, 1996). Poisson's ratio was determined for two orthogonal specimen orientations with respect to the applied load (ν_{13} and ν_{12}). These measurements showed very little difference between the two directions. We therefore assumed assume that $\nu_{12} \approx \nu_{32}$. The material can thus reasonably be considered as elastically isotropic for the numerical calculation of reference data ($\hat{K}_I(t)$ in Equation (2)). The measured mechanical properties are therefore: $E = 338$ GPa and $\nu = 0.3$.

4.2. Quasi-static fracture toughness – *KIc*

KIc determination was carried out along the guidelines of ASTM E399. This property was preliminarily determined to establish a reference for comparison with the dynamic values reported in this paper. The sample size was 11 *RL*, 14 *RR* and 4 *LR* specimens respectively. Two crosshead velocities were used: 0.5 mm min^{-1} and 10 mm min^{-1}, corresponding to typical stress intensity rates of 0.5 $MPam^{1/2}$ s^{-1} and 10 $MPam^{1/2}$ s^{-1}, respectively. The stress intensity rate is defined as the value of the stress intensity factor at fracture divided by the elapsed time. The results are listed in Table 1.

These results clearly indicate two facts. First, the quasi-static fracture toughness is moderately influenced by the loading rate, at least in the *RL* orientation. The sample size in the *LR* orientation is too small to identify a definite trend. Moreover, the quasi-static fracture toughness appears to be *relatively isotropic* considering the dispersion of the measured values. With these results, it is now interesting to assess the influence of the loading rate on the fracture toughness, both in terms of trends and absolute value.

4.3. Dynamic fracture toughness – *KId*

The dynamic fracture toughness was assessed using one point impact experiments (Weisbrod and Rittel, 2000). The sample size was 14 *RL*, 13 *RR* and 8 *LR* specimens respectively. All the specimens fractured without a shear lip. A representative fracture time, as recorded from specimen impact until the onset of crack propagation (Weisbrod and Rittel, 2000), was 16.5 μs for RL orientations and 21.5 μs for the *LR* and *RR* group. Here, the representative stress

Table 2. Dynamic fracture toughness – *KId* – for each orientation (the values have been rounded off to the nearest integer).

Stress intensity rate ($MPam^{1/2}\ s^{-1}$)	*RR* specimen ($MPam^{1/2}$)	*RL* specimen ($MPam^{1/2}$)	*LR* specimen ($MPam^{1/2}$)
$\sim 10^6$	89 ± 9	54 ± 7	92 ± 13

intensity rate was 10^6 $MPam^{1/2}\ s^{-1}$. The results for the various orientations are summarized in Table 2.

These results indicate a marked *anisotropy and rate sensitivity of the dynamic fracture toughness*.

4.4. Fractographic analysis

Characteristic crack-paths are shown for the various orientations in Figure 4. These views illustrate the relationship between the microstructure and the crack path, both at the initiation and near the tip of arrested cracks after impact. The crack-path is composed of the well known four components: tungsten-tungsten separation along a binding neck, cleavage of tungsten grain, tungsten-matrix interfacial separation and matrix failure (Churn and German, 1986; Couque et al., 1992). The last two mechanisms cannot be well discerned on the micrographs, but are easily identified by fractographic analysis. The relative occurrence of each failure mechanism is difficult to assess in order to pinpoint differences between the orientations. These micrographs also show the slight material anisotropy which correlates with the ovoidal shape of tungsten grains (*LR* and *RL* orientations). The crack-path at initiation cannot be assessed in a similar manner due to the large crack opening, by contrast with the vicinity of the arrested crack-tip.

Additional information of the fracture micromechanisms at initiation is presented in Figure 5. This observation complements the information shown in Figure 4, in which planes perpendicular to the crack path were shown. All the orientations disclose once again the 4 failure micromechanisms, without a marked dominance of either one in a specific orientation. By contrast with the *LR* and *RL* orientations, the *RR* orientation is now characterized by grains which are slightly elongated in a direction which is perpendicular to the crack-propagation direction.

5. Discussion

This study addresses two important issues related to fracture properties, which are seldom addressed for most engineering materials, and have not been previously reported for the tungsten base heavy alloys specifically.

The first issue concerns the anisotropy of the dynamic fracture properties, for a given and fixed alloy composition. While the the investigated material was found to be reasonably isotropic in terms of elastic moduli, the dynamic fracture toughness of the heavy alloy is nevertheless *anisotropic*, in sharp contrast with the quasi-static fracture toughness.

Our results also show that the fracture properties are *rate sensitive*. Once again, a marked difference is noted between the quasi-static and the dynamic fracture toughness of each ori-

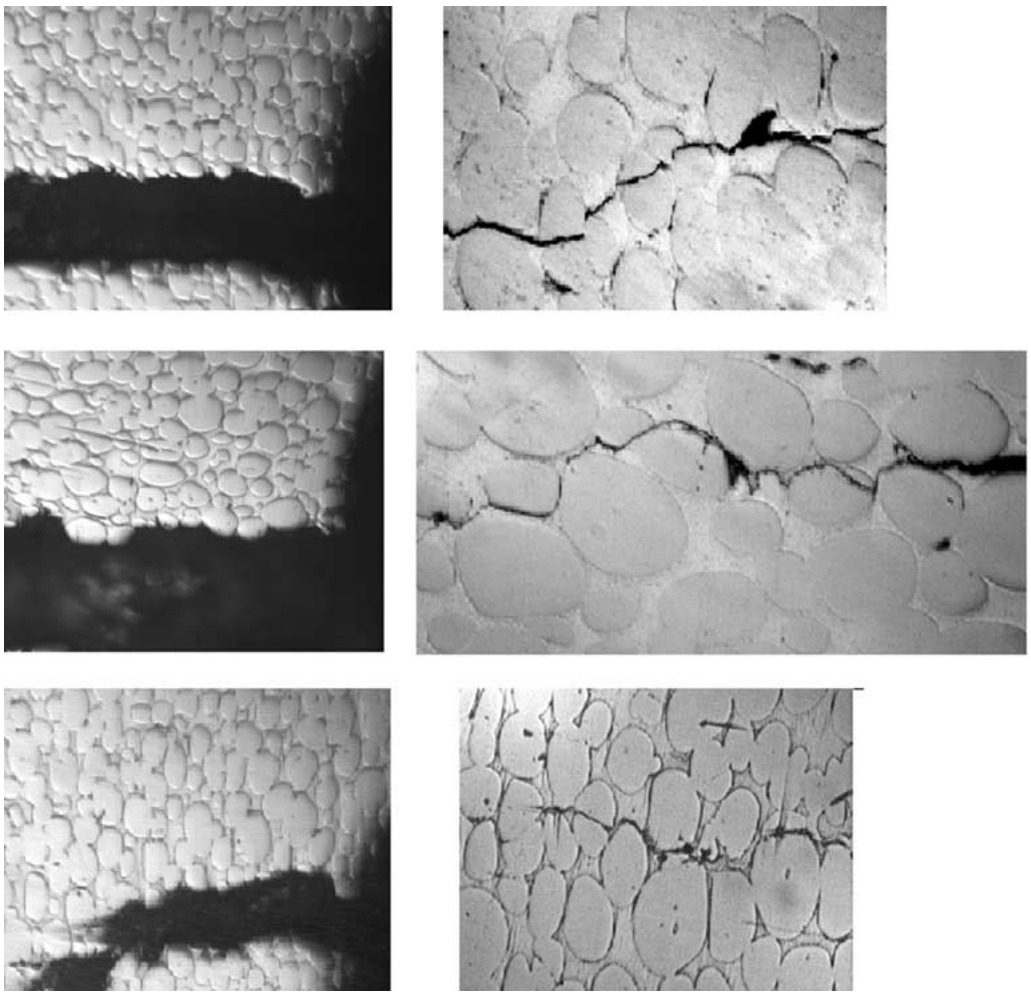

Figure 4. Dynamic fracture. Typical micrographs showing the fracture path close to the inititial notch (left hand-side) and near the arrested crack-tip (right handside). The specimens are as-polished. The characteristic failure mechanisms are outlined. Grain orientations can be correlated with Figure 2. (a) *RR* orientation, (b) *RL* orientation and (c) *LR* indication. CP indicates crack propagation.

entation. As mentioned previously, heavy alloys are known to exhibit strain rate sensitive mechanical properties. The degree of isotropy of the flow properties of the present alloy has not been characterized in this work. Nevertheless, the rate sensitivity of the fracture toughness is not totally surprising and has been mentioned in Couque et al. (1992). Further illustration of this result is given in Figure 6. Here the average static and dynamic values have been plotted as a function of the typical stress intensity rate. One additional important and new result appears in this figure: *the trend for toughness variations with the loading rate is not identical in all three orientations*. In fact, for the radially propagating cracks, the fracture toughness *increases* with the stress intensity rate. By contrast, for the longitudinally propagating cracks, the fracture toughness *decreases* with the stress intensity rate. This specific re sult is similar to that of Couque et al. (1992) who investigated several alloys with different thermomechanical histories.

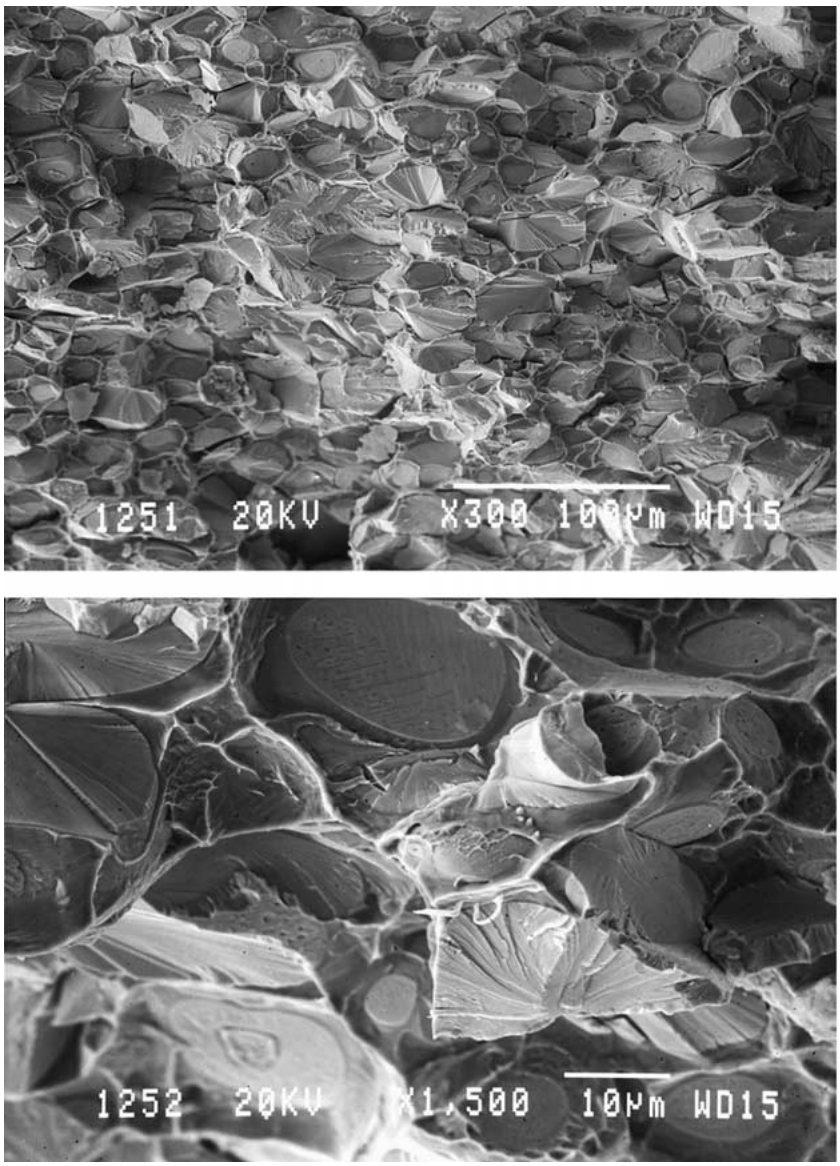

Figure 5. Dynamic fracture. Scanning electron fractographs of the three specimen orientations. Crack propagation from bottom to top of the pictures. Specific failure mechanisms have been outlined: W-W interface, cleavage of tungsten grain, matrix ductile failure. The tungsten-matrix interface is located adjacent to the W-W interface. (a) *RR* orientation, (b) *RL* orientation and (c) *LR* indication.

It was noted that the 'weaker' orientation exhibits smaller fracture time, on the average. The notion of 'fracture time', when all geometrical and impact parameters are left identical, has been used for dynamic fracture studies (dynamic key curves, Kalthoff et al., 1980). Our observations show an identical trend, but the method used here allows for variations in the loading parameters.

At this stage, one must assess the validity of the measured dynamic parameter. According to ASTM standards, the static yield strength value of 1450 MPa together with a representative toughness value of 90 MPam$^{1/2}$ yield a specimen thickness of 9.6 mm. This value is of the

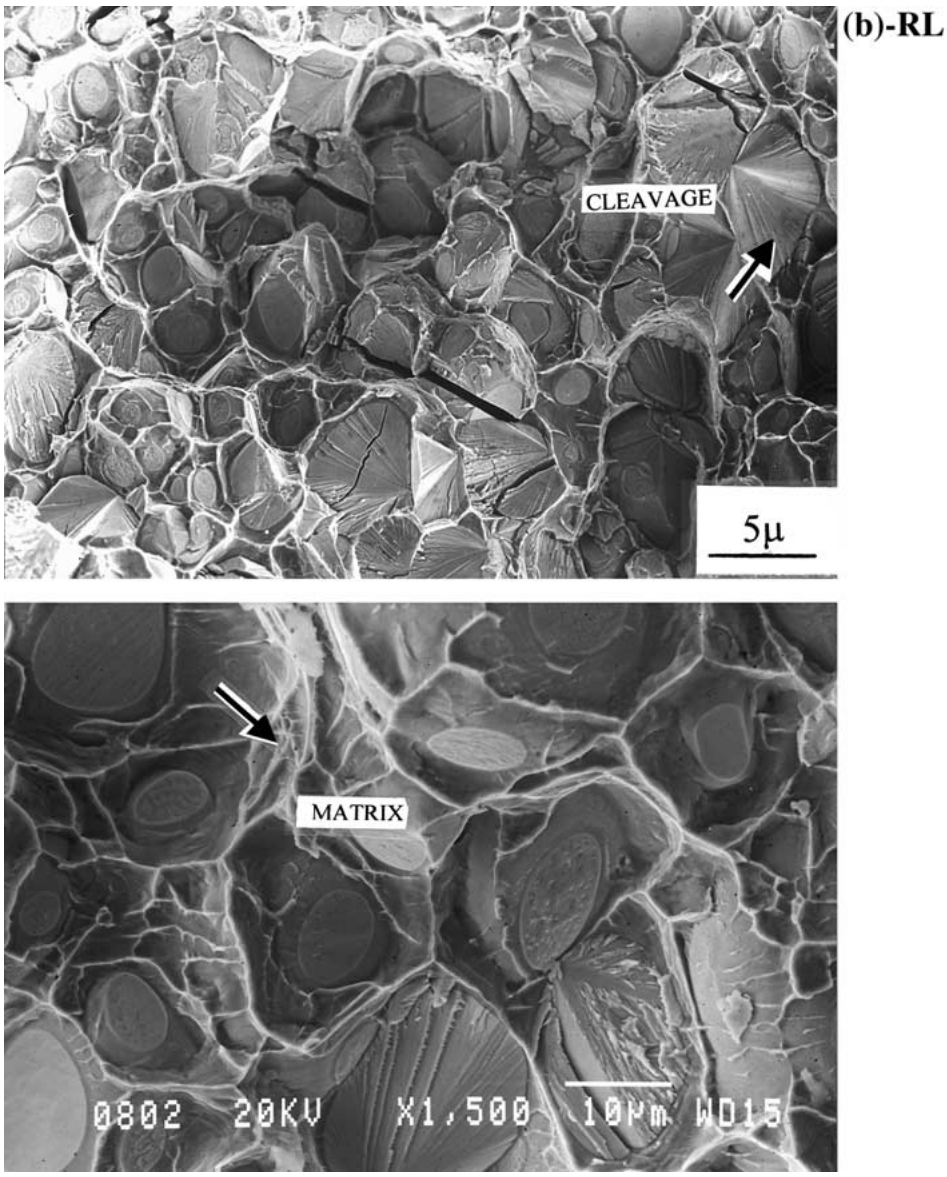

Figure 5. Continued.

order of the thickness of the present specimens (10 mm). Therefore, for static tests, the specimen thickness respects the recommendations of the standards. Keeping in mind the strain rate sensitivity of the material, the static yield strength value is likely to dictate a very conservative thickness value when dynamic testing is considered. Indeed the calculated thickness will be smaller if dynamic values of the yield stress are considered. Consequently, both the specimen thickness and the lack of shear lip indicate that the recorded values can be considered as valid, in the sense of the ASTM recommendations.

One additional delicate point remains the determination of the fracture time. This crucial issue sets the value of the fracture toughness, and it is determined by the fracture of the single wire fracture gages. This point has been discussed in detail in the description of the experimen-

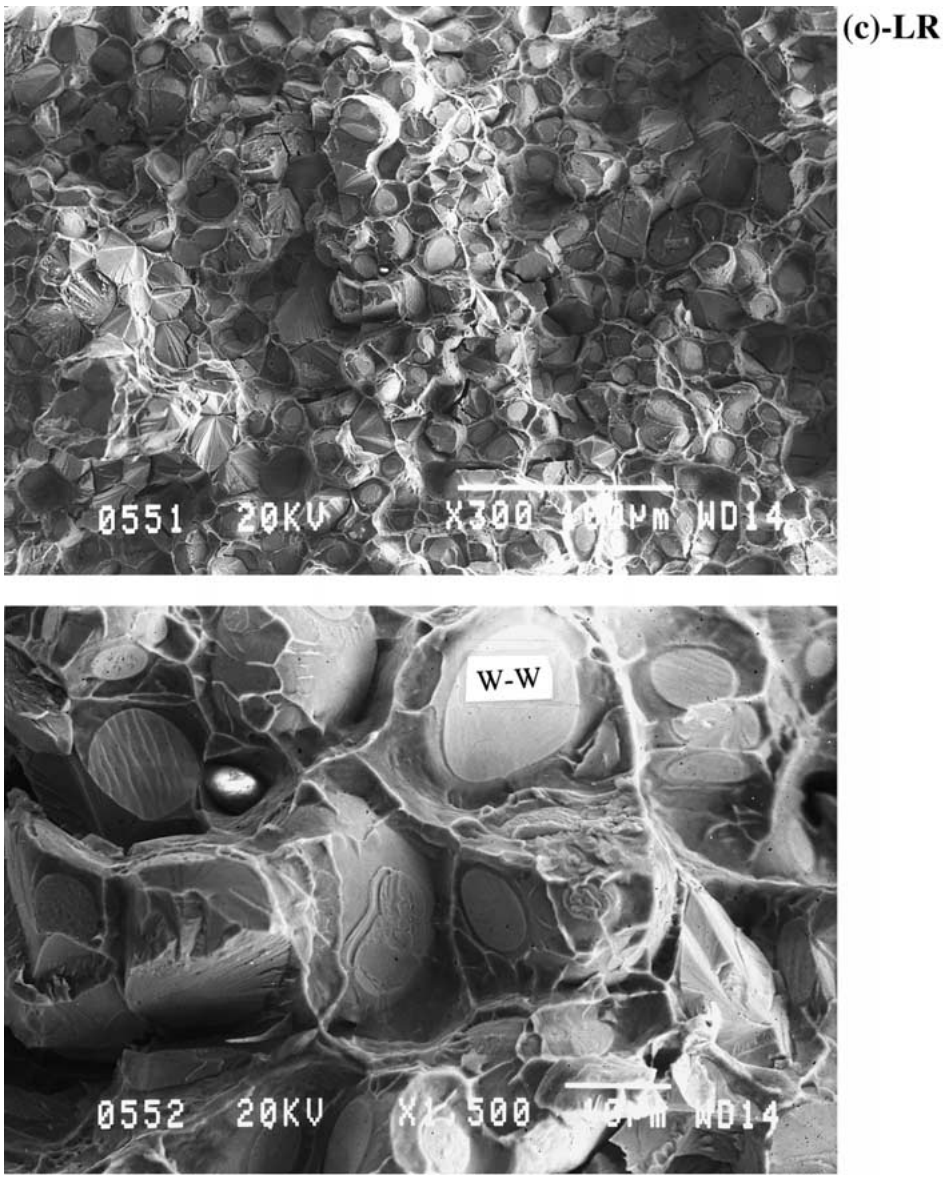

Figure 5. Continued.

tal method (Weisbrod and Rittel, 2000) and a very good agreement with crack-tip strain gage readings has been reported. As with our previously reported experiments, the fracture time was determined as the minimal value of the two fracture gage readings to ensure conservative results. Yet, while the overall accuracy in fracture time detection cannot exceed 1–2 μs, the observed *trend* for each group remains nevertheless valid since the same experimental error affects all the dynamic measurements, irrespective of the orientation.

However, the differences in dynamic fracture toughness, according to the orientation, are not clearly reflected at the microscopic scale. We did not observe a marked tendency for the dominance of a given failure mechanism, such as cleavage which is associated with a high fracture toughness fracture. It has been proposed that the rate sensitivity of the alloy could be

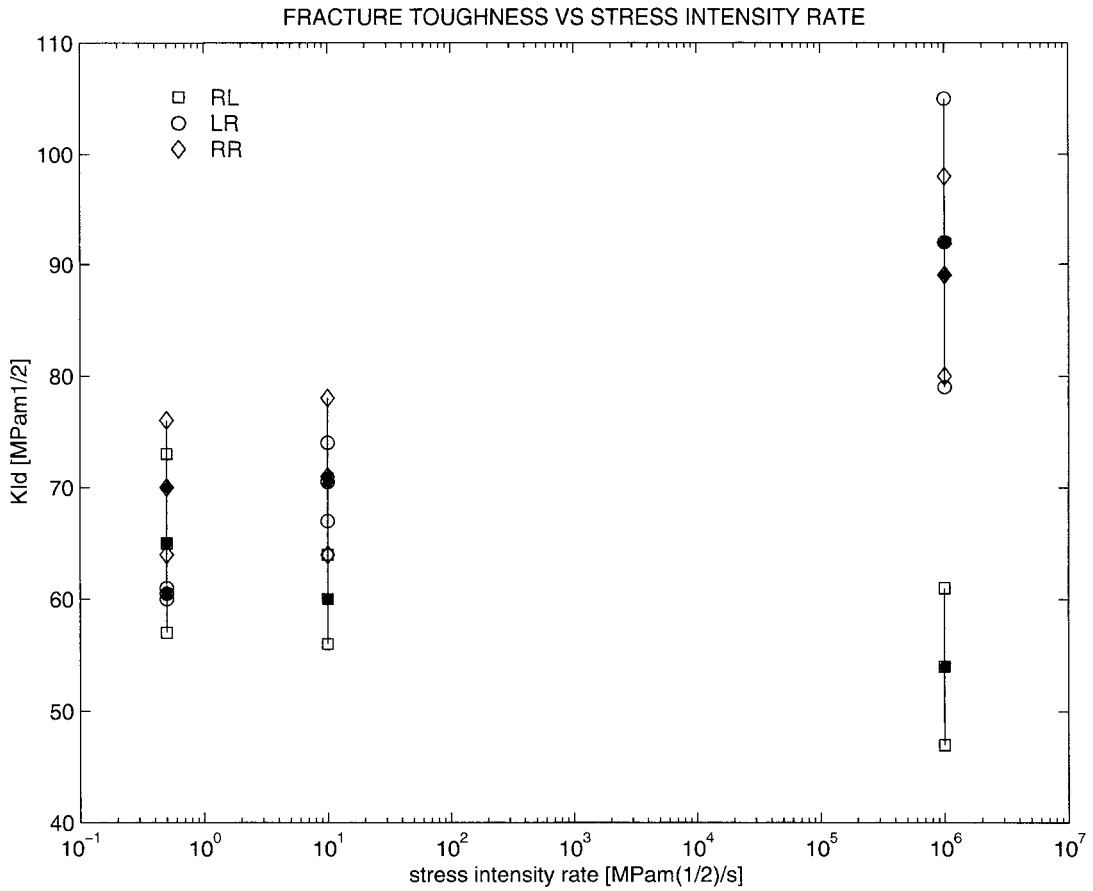

Figure 6. Fracture toughness as a function of the strain rate. The black symbols stand indicate the average result. The anisotropy and rate sensitivity of the fracture toughness is noticeable. Note the opposite trend for the rate sensitivity in *RR* and *LR* as opposed to *RL* orientations.

attributed to the BCC microstructure of the tungsten grains by contrast with the rate-insensitive FCC microstructure of the matrix phase (W-Ni-Fe) which surrounds the grains.

It thus appears that additional studies should be devoted to the following issues: quantitative description of each failure mode close to the initiation area, quantitative evaluation for the various fracture strengths (each failure mechanism at high strain rates), and the assessment of the degree of anisotropy of the dynamic mechanical properties (moduli and yield strength) of these alloys. These data could be incorporated in a micromechanical fracture model to improve our predictive capability regarding the (tensile) fracture properties of the heavy alloys.

6. Conclusions

- The static and dynamic fracture toughness of a swaged, commercial tungsten base heavy alloy have been studied in three distinct orientations (*LR, RL* and *RR*).
- The static and dynamic fracture properties of this material are different.
- The quasi-static fracture toughness is relatively isotropic and rate insensitive.
- By contrast, the dynamic fracture toughness is markedly anisotropic and rate sensitive.

- The variations of the dynamic fracture toughness depend on the orientation of the specimen and its crack.
- The dynamic fracture toughness of specimens with radially propagating cracks (*LR* and *RR*) *increases* with the loading rate.
- By contrast, the dynamic fracture toughness of specimens with longitudinally propagating cracks (RL) *decreases* with the loading rate.
- The variations in dynamic fracture fracture toughness are neither conclusively supported by fractographic examination, nor do they correlate with the apparent elastic isotropy of the investigated material.

References

Anderson, C.E., O'Donoghue, P.E., Bodner, S.R. (1988). Fracture of cubical tungsten specimens under explosive loading. *International Journal of Impact Engineering* **000**, 371–377.

ASTM (1993). Standard test method for plane-strain fracture toughness of metallic materials. *Annual Book of ASTM Standards*, Vol. 03.01.ASTM. Philadelphia, PA.

Broberg, K.B. (1999). *Cracks and Fracture*, Academic Press, NY, USA.

Couque, H., Lankford, J. and Bose, A. (1992). Tensile fracture and shear localization under high loading rate in tungsten alloys. *J. Phys. France* **2** 2225–2238.

Churn, K.S. and German, R.M. (1984). Fracture behavior of W-Ni-Fe alloys. *Met. Trans.* **15A**, 331–338.

Gurwell, W.E., Nelson, R.G., Dudder, G.B and Davis, N.C. (1984). *Fabrication and Properties of Tungsten Heavy Metal Alloys Containing 30% to 90% Tungsten*, US DOE Report DE-AC06-76RL0 1830.S

Hack, J.E. (1991). *Fracture Behavior of W based Materials*. Los Alamos National Laboratory Report 9-X68-9104V.

Kalthoff, J.F., Winkler, S., Böhme, W. and Klemm, W. (1980), Determination of the dynamic fracture toughness KId in impact tests by means of impact response curves. *Advances in Fracture Research*, (Edited by D. François et al.) Pergamon Press, New York, 363–373.

Kanninen, M.F. and Popelar, C.H. (1985). *Advanced Fracture Mechanics*. Oxford University Press. Oxford, U.K.

Kim, D.S., Nemat-Nasser, S., Isaacs, J.B. and Lischer, D. (1998). Adiabetic shearband in WHA in high strain-rate compression. *Mechanics of Materials* **28**, 227–236.

Krock, R.H. and Shepard, L.A. (1963). Mechanical behavior of the two phase composite, Tungsten-Nickel-Iron. *Transactions AIME* **277**, 1127–1134.

Nye, J.F. (1957). *Physical Properties of Crystals*. Oxford University Press, Oxford, U.K.

Ostolaza Zamora, K.M., Gil Sevillano, J. and Fuentes Perez, K. (1992). Fracture toughness of W heavy metal alloys. *Materials Science and Engineering* **A157**, 151–160.

Ramesh, K.T. and Coates, R.S. (1992). Microstructural influences on the dynamic response of tungsten heavy alloys. *Met. Trans.* **23A**, 2625–2630.

Rittel, D. and Roman, I. (1986). Ductility and precipitation in sintered tungsten alloys. *Materials Science and Engineering* **A82**, 93–99.

Rittel, D. and Maigre, H. (1996). An investigation of dynamic crack initiation in PMMA. *Mechanics of Materials* **26**, 229–239.

Wada, H. (1992). Determination of dynamic fracture toughness for PMMA. *Eng. Fract. Mech.* **41**, 821–831.

Weisbrod, G. and Rittel, D. (2000). A method for dynamic fracture toughness determination using short beams. *International Journal of Fracture* **104**, 89–103.

Woodward, R.L., Baldwin, N.J., Burch, I. and Baxter B.J. (1985). Effect of strain rate on the flow stress of three liquid phase sintered tungsten alloys. *Met. Trans.* **16A**, 2031–2037.

Zurek, A.K. and Gray, G.T. (1991). Dynamic strength and strain rate effects on fracture behavior of tungsten and tungsten alloys. *Colloque C3 J. de Physique III* **1**, 631–637.